https://doi.org/10.5194/acp-2021-814
Preprint. Discussion started: 26 October 2021

Atmospheric Chemistry and Physics Discussions

Influence of Photochemical Loss of VOCs on Understanding Ozone Formation Mechanism

Wei Ma[1], Zemin Feng[1], Junlei Zhan[1], Yongchun Liu[1*], Pengfei Liu[2,4,5], Chengtang Liu[2,4,5], Qingxin Ma[2,4,5], Kang Yang[3], Yafei Wang[3], Hong He[2,4,5], Markku Kulmala[1,6], Yujing Mu[2,4,5], Junfeng Liu[2,4,5*]

1. Aerosol and Haze Laboratory, Advanced Innovation Center for Soft Matter Science and Engineering, Beijing University of Chemical Technology, Beijing, 100029, China

2. Research Center for Eco-Environmental Sciences, Chinese Academy of Sciences, Beijing, 100085, China

3. Beijing Institute of Petrochemical Technology, Beijing 102617, China

4. Center for Excellence in Regional Atmospheric Environment, Institute of Urban Environment, Chinese Academy of Sciences, Xiamen 361021, China

5. University of Chinese Academy of Sciences, Beijing 100049, China

6. Institute for Atmospheric and Earth System Research, Faculty of Science, University of Helsinki, Helsinki, 00014, Finland

*Corresponding to: Yongchun liu (liuyc@buct.edu.cn) and Junfeng Liu (junfengliu@rcees.ac.cn)

https://doi.org/10.5194/acp-2021-814
Preprint. Discussion started: 26 October 2021

Atmospheric Chemistry and Physics Discussions

Abstract

Volatile organic compounds (VOCs) tend to be consumed by atmospheric oxidants, resulting in substantial photochemical loss during transport. An observation-based model is used to evaluate the influence of photochemical loss of VOCs on the sensitivity regime and mechanisms of ozone formation. Our results showed that a VOC-limited regime based on the observed VOC concentrations shifted to a transition regime with the photochemical initial concentration of VOCs (PIC-VOCs) in the morning. The net ozone formation rate was underestimated by 3 ppb h^{-1} (36 ppb day^{-1}) based on the PIC-VOCs. The relative contribution of the RO_2 path to ozone production based on the PIC-VOCs accordingly increased by 13.4%, particularly, the contribution of alkenes derived RO_2 increased around 10.2%. The contribution of local photochemistry might be underestimated to both local and regional ozone pollution if the consumed VOCs was not accounted for, and policy-making on ozone pollution prevention should focus on high-reactivity VOCs.

https://doi.org/10.5194/acp-2021-814
Preprint. Discussion started: 26 October 2021

1. Introduction

Ground surface ozone (O_3) is an important atmospheric pollutant that is harmful to human health, such as connecting with respiratory, cardiovascular diseases and premature mortality (Cohen et al., 2017). It is also harmful to vegetation growth. For example, it led to annual reduction of the yield of rice and wheat by 8% and 6%, respectively, and the forest biomass growth by 11-13% in China (Feng et al., 2019). Surface O_3 concentrations have increased by 11.9% over eastern China under the air pollution control measures implemented in China from 2012 to 2017 (Dang and Liao, 2019). An economic loss will be 0.09% of the Chinese gross domestic products (78 billion CNY) in 2030 if the policies against O_3 pollution are not properly implemented (Xie et al., 2019). Therefore, it is urgent to take actions on O_3 pollution in China.

Tropospheric O_3 is mainly produced from photochemical reactions between volatile organic compounds (VOCs) and nitrogen oxides (NO*x*: NO+NO_2) (Seinfeld and Johnh, 2006; Zhang et al., 2021c). O_3 is generated from the collision of O_2 and O(3P) that are produced from the photolysis of NO_2 in the atmosphere. Peroxyl radicals (HO_2 and RO_2), which produced from oxidation of VOCs by OH radical, can efficiently convert NO (from the photolysis of NO_2) to NO_2, then lead to net O_3 production by compensating the titration of O_3 by NO(Monks, 2005; Zhang et al., 2021a). Over past two decades, a number of field observations focused on the pollution level of O_3 and its precursors have been carried out in Beijing-Tianjin-Hebei (BTH), the Yangtze River Delta (YRD), and Pearl River Delt (PRD) regions (Wang et al., 2017; Li et al., 2019; Xue et al., 2014; Zhang et al., 2019). Due to the nonlinear relationship between O_3 and its precursors and the variations of meteorological conditions, numerous studies have

https://doi.org/10.5194/acp-2021-814
Preprint. Discussion started: 26 October 2021

been performed for understanding the sensitivity regime (Ling and Guo, 2014; Zhang et al., 2020) and the photochemical process of O_3 formation based on box model or observation-based model (OBM) (He et al., 2019; Tan et al., 2019), and the source-receptor relationship of O_3 using a regional chemical transport mode (Li et al., 2016b; Li et al., 2016c). Recently, O_3 formation process, from the perspective of the instantaneous production rate, has attracted more attention, such as the radical recycle (OH-RO_2-RO-HO_2-OH) relating to production of O_3 (Lu et al., 2017; Tan et al., 2017; Whalley et al., 2018). It has been found that HCHO photolysis and alkene ozonolysis contributed about 85 % of the primary production of HO_2 and HO radicals in Beijing, Shanghai and Guangzhou (Tan et al., 2019; Yang et al., 2017). The importance of HONO and HCHO photolysis for primary radical production has also been proposed in suburban and rural areas (Tan et al., 2017; Lu et al., 2012; Lu et al., 2013).

It should be pointed out that all of the OBM studies were based on the measured dataset when investigating the relationship between O_3 and VOCs. However, VOCs is highly reactive to atmospheric oxidants, such as OH, NO_3, and O_3, in which OH is the dominant one. The lifetimes of some highly reactive VOCs such as isoprene are only as short as several ten minutes under the typical daytime atmospheric conditions. Thus, the mixing ratio of VOCs observed at a sampling site may differ from that at the source regions because of the photochemical loss even during a short-range of transport. This may mislead the O_3 formation sensitivity, net O_3 production, subsequently, the policy-making on O_3 pollution prevention. Thus, the photochemical-age-based approach has been applied to evaluate the effect of photochemical process on VOC measurements (Shao et al., 2011). This method was used to qualitatively or

https://doi.org/10.5194/acp-2021-814
Preprint. Discussion started: 26 October 2021

semi-quantitatively estimate the O_3 formation process of the source-receptor (Gao et al., 2018), such as calculating O_3 formation potential (OFP) (Han et al., 2017), identifying the critical species for O_3 formation (Gao et al., 2021), and evaluating the VOCs emission ratio (Yuan et al., 2013). However, it is unclear how the highly reactive VOCs, which has degraded during transport from the source to the receptor site, will affect the instantaneous formation process of O_3.

In this study, an OBM is used to evaluate the local O_3 formation process in summer in Beijing based on the concentrations of the observed and photochemical initial concentrations of VOCs (PIC-VOCs). The O_3-NO*x*-VOCs sensitivity, the instantaneous O_3 formation rate and the in-situ O_3 formation process are discussed. The aim of this study is to understand the possible influence of photochemical loss of VOCs on the diagnosis of the formation sensitivity regime of O_3. This study can provide a new insight for better understanding atmospheric O_3 pollution.

2. Methodology

2.1 Experimental section

Field observations were carried out in the Qingyuan campus of Beijing Institute of Petrochemical Technology (BIPT, 39.73°N and 116.33°E) (Figure S1). The details about the observation site has been described in our previous work (Zhan et al., 2021). Briefly, the site is a typical suburb site in Daxing District between the 5th ring road and the 6th ring road. The field campaign was carried out during August 1st-28th in 2019 when photochemistry was the most active while rainfall was rare in Beijing.

https://doi.org/10.5194/acp-2021-814
Preprint. Discussion started: 26 October 2021

The concentrations of non-methane hydrocarbons (NMHCs) were detected by both a gas chromatography-flame ionization detector (GC/FID) and a single photon ionization (SPI) TOF-MS (SPI-MS 3000, Guangzhou Hexin Instrument Co., Ltd., China). A detailed description of instrumentation can be found in previous publications (Zhan et al., 2021; Chen et al., 2020). The SPI-MS was also deployed to detect halohydrocarbons. More details of this instrument and the parameter-setting have been described in previous studies(Zhang et al., 2019; Liu et al., 2020a).. Briefly, a polydimethylsiloxane (PDMS; thickness of 0.002 int; Technical Products Inc., USA) membrane was used to gathering VOCs and diffuse from the sample side to the detector side under high vacuum conditions. A vacuum ultraviolet (VUV) light generated by a commercial D2 lamp (Hamamatsu, Japan) was utilized for ionization at 10.8 eV. For ion detection, two microchannel plates (MCPs, Hamamatsu, Japan) assembled with a chevron-type configuration are employed. This TOF-MS has an LOD varied from 50 ppt to 1 ppb with 1 minute of time resolution for most trace gases without any pre-concentration procedure. To verify the data compatibility of the SPIMS and GC/FID, we compared the concentrations of toluene measured using these two different instruments (Figure S2). The correlation coefficient is 0.92, indicating that the concentrations of NMHCs are comparable using these two measurement techniques.

Oxygenated VOCs (OVOCs) were collected and analyzed using a high-performance liquid chromatography (HPLC, Inertsil ODS-P 5 μm 4.6 × 250 mm column, GL Sciences) with acetonitrile-water binary mobile phase(Ma et al., 2019). OVOCs were collected into 2,4-dinitrophenylhydrazine (DNPH)-coated silica gel cartridges (Sep-Pak, Waters) by an automatic

https://doi.org/10.5194/acp-2021-814
Preprint. Discussion started: 26 October 2021

sampling device, with the sampling flow rate of 1.2 L min-1 and the duration of 2 h for each sample. To avoid possible contamination or desorption after sampling, cartridges were capped, placed into tightly closed plastic bags and kept in a refrigerator before analysis. The sampled cartridges were eluted by 5 mL acetonitrile and analyzed by HPLC as soon as possible after they were shipped back to the laboratory. This system was calibrated through 8-gradient standard solutions (TO11/IP-6A Aldehyde/Ketone-DNPH Mix, SUPELCO). The correlation coefficients were all greater than 0.999. The LOD for most OVOCs is about 10 ppt.

Trace gases, including NO*x*, SO_2, CO, and O_3, were measured using the corresponding analyzer (Thermo Scientific, 42i, 43i, 48i, and 49i, respectively). The HONO concentration was measured using a home-made long path absorption photometer (LOPAP) (Liu et al., 2020c). The meteorological parameters, including temperature (T), pressure (P), relative humidity (RH), wind speed, and wind direction, were measured using a weather station (AWS310, Vaisala). The photolysis rate (J_{NO2}) was measured via a continuous measurement of the actinic flux in the wavelength range of 285-375 nm using a J_{NO2} filter-radiometer (J_{NO2} radiometer, Metcon).

2.2 Calculation of photochemical loss of VOCs.

The photochemical loss of VOC was calculated using the ratio method (Wiedinmyer et al., 2001; Yuan et al., 2013). The initial mixing ratio of a specific VOC was calculated using the equations(Mckeen et al., 1996):

$$[VOC_i]_t = [VOC_i]_{t0} \times \exp(-k_i \times [OH] \times \Delta t) \quad (1)$$

$$\Delta t = \frac{1}{[OH]\times(k_X - k_E)} \times \left\{ ln\left(\frac{X_0}{E_0}\right) - ln\left(\frac{X_t}{E_t}\right) \right\} \quad (2)$$

https://doi.org/10.5194/acp-2021-814
Preprint. Discussion started: 26 October 2021

where $[VOC_i]_t$ and $[VOC_i]_{t0}$ are the observation concentration and the initial concentration of VOC_i; k_i is the second-order reaction rates between the compound i and $[OH]$; $[OH]$ and Δt are the concentration of OH radical and photochemical aging time, respectively. k_X and k_E are rate constant for the reaction between OH radicals and xylene (7.00×10^{-12} cm^3 molecule^{-1} s^{-1}) and ethylbenzene (1.87×10^{-11} cm^3 molecule^{-1} s^{-1}) (Atkinson and Arey, 2003), respectively. (X_0/E_0) is the ratio between the initial xylene and ethylbenzene mixing ratios, and (X_t/E_t) is the ratio between the observed xylene and ethylbenzene mixing ratios at time. In this study, we chose the mean concentrations of xylene and ethylbenzene at 05:00-06:00 as the initial concentrations (no photochemical loss) to calculate the photochemical loss of OH exposure. As can be seen from Figure S3, the concentrations of xylene and ethylbenzene are well correlated, which indicates that they are homologous emitted simultaneously. The calculated OH exposure ($[OH]\times\Delta t$) was $4.3\pm1.9\times10^6$ molecule cm^{-3} h. Accordingly, the mean photochemical ages were 1.7 $\pm$0.9 h using the mean daytime (8:00-17:00 LT) OH concentrations ($4.3\pm3.1\times10^6$ molecules cm^{-3}) estimated using our previous method (Liu et al., 2020b; Liu et al., 2020c). This means that the VOCs would undergo obvious degradation even in a short-range of transport in the atmosphere.

It should be noted that the k_{OH} of isoprene is 9.98×10^{-11} cm^3 molecule^{-1} s^{-1} at 298.15 K (Atkinson and Arey, 2003), almost two orders than other VOCs. The ratio method assumes constant emissions for VOCs. However, the emission of isoprene greatly depends on temperature and solar irradiation intensity (Zhang et al., 2021b). Besides the photochemical loss, additional correction of daytime isoprene concentrations was performed using the average

https://doi.org/10.5194/acp-2021-814
Preprint. Discussion started: 26 October 2021

diurnal flux of isoprene emissions (Figure S4) (Zhang et al., 2021b). The emission of isoprene shows a clear unimodal curve, and the volume concentration of isoprene is calculated based on the daily emission curve using Eq. (S1).

2.3 Observation-based model simulation

A box model based on the Master Chemical Mechanism (MCM3.3.1) and the Regional Atmospheric Chemical Mechanism (RACM2) were used in this study. The MCM3.3.1 was used to understand the instantaneous ozone formation process, and the RACM2 was used to depict the ozone isopleth due to the high computational efficiency (Sect. 2.4). Table S1 shows the model inputs. The model calculation is constrained with the measured meteorological parameters (RH, T, P, and J_{NO2}) and the concentrations of trace gases, including inorganic species (NO, NO_2, CO, SO_2, and HONO) and 61 organic species (NMHCs (46), OVOCs (8), and halohydrocarbons (7)). The model was validated using the observed and simulated O_3 concentrations, which showed good consistency as shown in Figure. S5. The slope and correlation coefficient were 0.90 and 0.82 (Figure. S6), respectively, indicating the rationality of model simulation.

The ozone formation rate $P(O_3)$ can be quantified by the oxidation rate of NO to NO_2 by peroxyl radicals (Tan et al., 2019), as expressed in Eq. (3). In this study, the modeled peroxyl radical concentrations are used to calculate the ozone production rate.

$$P(O_3) = k_{HO_2+NO}[HO_2][NO] + k_{RO_2+NO}[RO_2][NO] \quad (3)$$

where $P(O_3)$ is the ozone formation rate; $[HO_2]$and $[RO_2]$ are the number concentrations of HO_2 and RO_2 radicals; k_{HO2+NO} and k_{RO2+NO} are the second reaction rates between the HO_2 and

https://doi.org/10.5194/acp-2021-814
Preprint. Discussion started: 26 October 2021

RO_2 and NO. Once ozone formed, it will be consumed by OH, HO_2, and alkenes. Also, a part of NO_2 can react with OH, resulting in the formation of nitrate before photolysis. The chemical loss of both O_3 and NO_2 is considered in the calculation of the net ozone production rate (Tan et al., 2019),

$$\mathrm{L}(O_3) = \left(k_{O_3+OH}[OH] + k_{O_3+HO_2}[HO_2] + k_{O_3+alkenes}[alkenes]\right)[O_3] + k_{NO_2+OH}[NO_2][OH] \quad (4)$$

where $L(O_3)$ is the ozone chemical loss rate; $[HO]$ is the number concentration of HO radical; k_{O3+OH}, k_{O3+HO2}, and $k_{O3+alkenes}$ are the second reaction rate between the O_3 and OH, HO_2 and alkenes, respectively; and k_{NO2+OH} is the second reaction rate between the NO_2 and OH. Finally, $F(O_3)$ is the net ozone formation rate by the difference between the $P(O_3)$ and $L(O_3)$ as expressed in Eq. (5),

$$\mathrm{F}(O_3) = \mathrm{P}(O_3) - \mathrm{L}(O_3) \quad (5)$$

2.4 Empirical Kinetic Modeling Approach

The empirical kinetic modeling approach (EKMA) used in this work is a set of imaginary tests to reveal the dependence of photochemical oxidation products on the change in precursors. We set up 30 × 30 matrixes by reducing or increasing the measured VOCs and NO*x* concentrations to the model input. The resulting radical concentrations and ozone production rates are calculated correspondingly.

In this stage, the observed VOCs are grouped into different parcels according to the classification of RACM2, and more details can be found in the previous publication (Tan et al., 2017). The chemical model simulates the photochemical reactions with the parameters at a

https://doi.org/10.5194/acp-2021-814
Preprint. Discussion started: 26 October 2021

time interval of 5 minutes, which is enough for the NO, NO_2, OH, HO_2, and RO_2 reaching steady state due to the typical relaxation time of the chemical system is 5-10 minutes in summer (Tan et al., 2018). The ozone production rate is calculated as described in Sect. 2.3.

3. Results and discussion

3.1 Overview of diurnal variation of O_3, NO*x*, TVOC

Figure 1 shows the average diurnal variation of O_3, NO*x*, and TVOCs (includes alkanes, alkenes, OVOCs, and halohydrocarbons), driven by the emissions, photochemical reactions and the evolution of the mixing layer height (MLH). The ozone concentration during the observation period was 44.8±27.2 ppb with a maximum of 119.1 ppb as reported in our previous study (Zhan et al., 2021), which is generally comparable with the O_3 concentrations during 2014-2018 (Ma et al., 2020). O_3 followed a unimodal curve with a minimum (18.8±15.4 ppb) at 07:00, then increased to the maximum (69.6 ppb) at 15:00 as photochemical ozone formation. On the contrary, NO*x* was up to the maximum concentration (39.7±14.2 ppb) at 07:00, and then decreased. After 07:00, the mixing ratio of NO went down all the time, while the concentration of NO_2 decreased at first, while started to grow at 14:00. The diurnal variations of the observed TVOCs were generally consistent with NO_2. The observed TVOCs concentrations ranged from 2.2 to 23.2 ppb, with a mean value of 18.6±2.6 ppb. Compared to the same period (45.4±15.2 ppb) in August 2015 (Li et al., 2016a), the concentration of VOCs in Beijing has been effectively reduced. However, the photochemical initial concentrations (PICs) of TVOCs, which varied from 2.2 to 31.2 ppb with a mean value of 22.4±3.8 ppb, showed a different diurnal curve compared with the observed one. It slightly increased from

https://doi.org/10.5194/acp-2021-814
Preprint. Discussion started: 26 October 2021

14:00 to 17:00, which is similar with the diurnal variation of the VOCs in previous work (Zhan et al., 2021). The daytime PIC-VOCs was 7.7±0.46 ppb higher than the observed concentration of TVOCs, indicating an underestimated contribution of local photochemistry of VOCs to O_3 and organic aerosol formation.

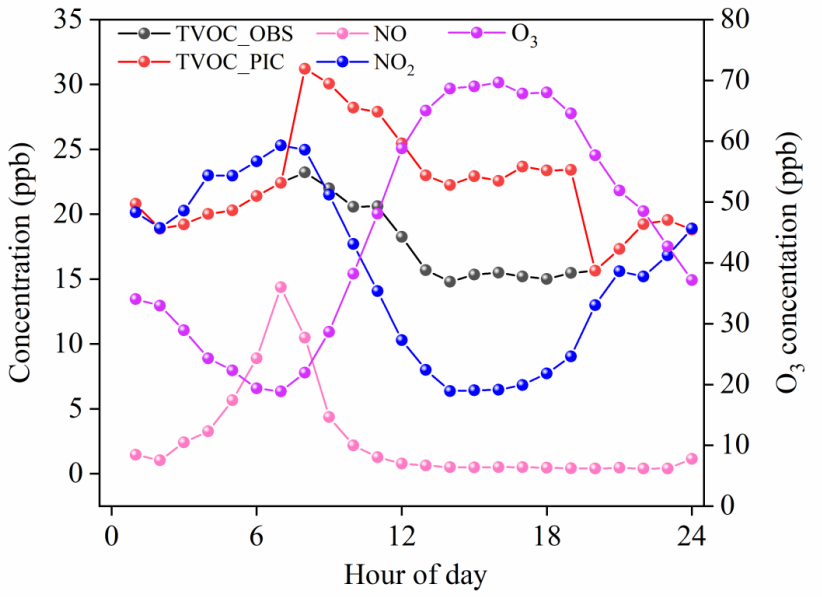

Figure. 1. Overview of diurnal variations of O_3, NO*x*, and TVOC

3.2 Influence of photochemical loss of VOCs on O_3 formation sensitivity regime

The sensitivity of O_3 formation is analyzed using the isopleth diagram which was generated from the EKMA model, which is widely use to study O_3-NO*x*-VOCs sensitivity qualitatively. As described in Sect. 2.4, the concentrations of NO_2 and VOCs were artificially scaled ±75% of the observed values to disclose the response of O_3 concentration to an imaginary change in the concentrations of NO_2 and VOC with other constrained conditions unchanged. Figure. 2 shows the typical EKMA curves during our observations. The black full

https://doi.org/10.5194/acp-2021-814
Preprint. Discussion started: 26 October 2021

star and pentagon denote the observed concentrations of NO*x* and VOCs in the morning and at noon, respectively, while the blue symbols are the corresponding values of PICs. Based on the measured data, the O_3 formation was in a VOCs-limited regime in the morning and a NO*x*-limited regime at noon. The black arrow indicated a linearly decreasing trend of NO*x* and VOCs from 08:00 to 15:00 in the chemical coordinates system, and the ozone production shifted from VOC-limited to NOx-limited conditions from morning to noon, which was consistent with the mean diurnal profiles (Figure. 1). This is similar to that reported in Wangdu (Tan et al., 2018). As expected, the ozone production shifted from a VOC-limited regime (the observed VOCs) to a transition one based on the PIC-VOCs in the morning. It further obviously moved to a NO*x*-limited regime at noon after the photochemically consumed NO*x* and VOCs had been accounted for (Figure. 2). These results denoted that the O_3 formation mechanism might be misdiagnosed, misleading the mitigation measures for O_3 prevention if not considering the consumed VOCs in the real atmospheric condition because the average photochemical aging time was only 1.7±0.9 h.

https://doi.org/10.5194/acp-2021-814
Preprint. Discussion started: 26 October 2021

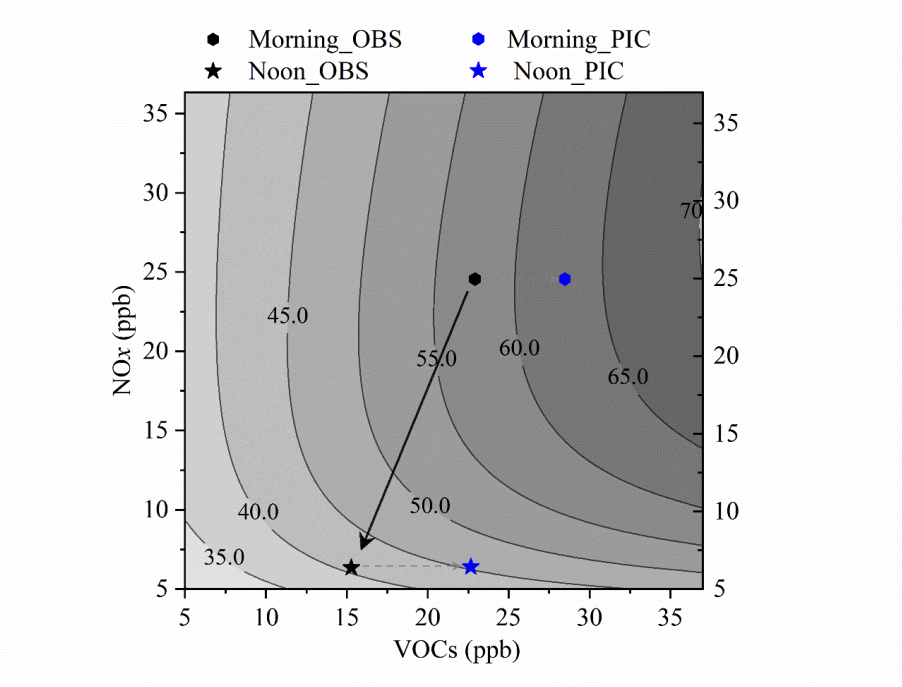

Figure 2. Isopleth diagram of the ozone concentration as functions of the concentration of NO*x* and VOCs derived from an empirical kinetic modeling approach. The pentagons and starts indicate the status in the morning and at noon, respectively. The black-filled and blue filled are the observed and corrected status, respectively.

3.3 Contribution of VOC species to O_3 production

The time series of simulated OH, HO_2, and RO_2 concentrations are used to calculate the $P(O_3)$ and $L(O_3)$. The diurnal averaged $P(O_3)$ and $L(O_3)$ are shown in Figure 3. The ozone formation can be divided into RO_2+NO and HO_2+NO related processes (Sect. 2.3). According to VOC precursors, the peroxyl radical groups are divided into alkane-derived (ALKAP), alkene-derived (AlKEP), aromatic-derived (AROMP), isoprene-derived (ISOP), oxygenated-VOC-derived (OVOCP), and halohydrocarbon-derived (HALOP) RO_2 and HO2P. The ozone destruction processes include the reaction between O_3 and HO*x* (O3D1), the reaction between O1D and H_2O (O3D2), alkenes (O3D3), and the reaction between NO_2 and OH (O3D4).

https://doi.org/10.5194/acp-2021-814
Preprint. Discussion started: 26 October 2021

Based on the observed VOCs (or PIC-VOCs), the fast O_3 production rate was observed at 14:00 (or 13:00), with a diurnal maximum value of 16.1 (or 25.6) ppb h^{-1} (Figure 3a and 3b), while the peaked destruction rate was 6.4 (or 8.6) ppb h^{-1} at 15:00 (or 13:00) (Figure 3c and 3d). The average daytime $P(O_3)$ based on the initial concentrations of VOCs was 4.0±3.1 ppb h^{-1} higher than that based on the measured concentrations (Figure 3b). At the same time, the $F(O_3)$ based on the initial concentrations of VOCs was also 3.0±2.1 ppb h^{-1} higher than the counterpart (Figure S7). Thus, the net O_3 production can accumulatively be underestimated by 36 ppb day^{-1} if the consumption of VOCs was not considered. This means the contribution of local formation of O_3 should be underestimated using the directly measured VOCs concentrations.

The HO_2 path contributed 64.8% to the total ozone formation on average, which is slightly higher than the reported value (57.0%) in Wangdu (Tan et al., 2018); whereas, the RO_2 path contributed to the rest part, in which aromatics (9.4%), alkenes (8.4%), isoprene (7.8%), alkanes (4.7%), OVOCs (4.3%) and halohydrocarbons (0.6%) were the main contributors. As for the PIC-VOCs, the dominant path of production of O_3 (51.7%) was still the HO_2 path, followed by the RO_2 path related to alkenes (14.7%), aromatics (12.8%), and isoprene (11.7%). The relative contribution of the RO_2 path to $P(O_3)$ increased by 13.4% compared with the measured-VOCs, particularly alkenes derived RO_2 increased 10.2%. As shown in Figure 3c and 3d, the destruction of total oxidants was dominated by the reaction between O_3 and alkenes (O3D3) in the morning. It gradually shifted to the reaction between NO_2 and OH (O3D4) from 11:00 to 16:00, the photolysis of O_3 followed by reaction with water (O3D2) from 12:00 to

https://doi.org/10.5194/acp-2021-814
Preprint. Discussion started: 26 October 2021

15:00 because O_3 concentration increased while NO_2 decreased (Figure 3c). The O_3 destruction of HO*x* and O_3 reaction (O3D1) gradually increased with the continuous photochemical reaction. In addition, the maximum O_3 formation rate of the RO_2 derived from OVOCs and halohydrocarbons were 0.75 and 0.18 ppb h^{-1}. These values could be underestimated due to the incomplete gas reaction mechanism of OVOCs and halohydrocarbons in the MCM3.3.1. In general, the measured VOCs as model input could not truly reflect the oxidation capacity and underestimate the local formation of O_3 and organic aerosol (Zhan et al., 2021).

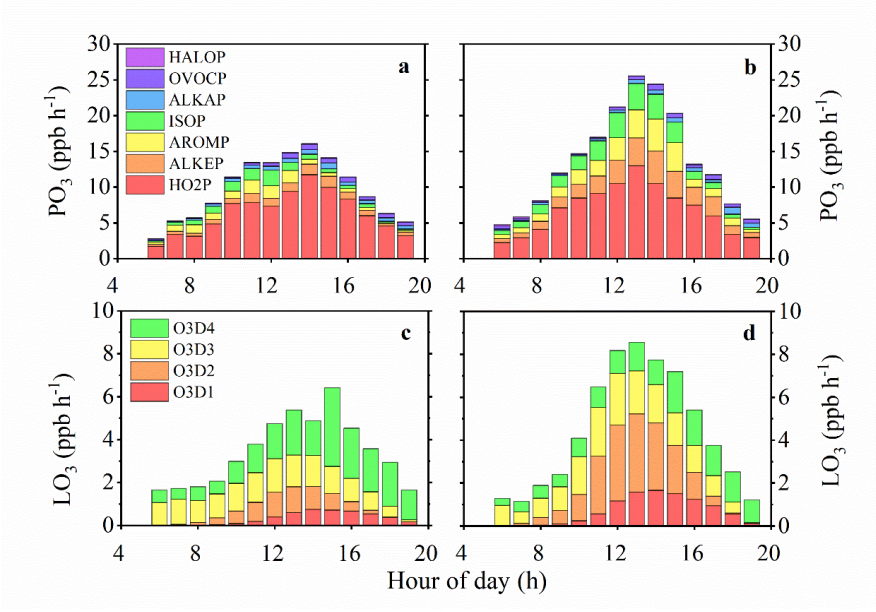

Figure 3. Mean diurnal profile of the instantaneous ozone production and destruction rate calculated from the MCM-OBM model (instantaneous ozone rate derived from observed VOCs in a and c, and from PIC-VOCs in b and d). The upper panel presents the speciation ozone formation rate. The lower panel presents the speciation ozone destruction rate.

The budget of OH-HO_2-RO_2 radicals was further analyzed to understand the photochemical O_3 formation process. All radical cycles are divided into four groups (source, sink, propagation, and equilibrium between radical and reservoir species) based on the different

https://doi.org/10.5194/acp-2021-814
Preprint. Discussion started: 26 October 2021

radical reaction processes (Tan et al., 2019). The comparison of radical budget derived from the observed and PIC-VOCs is shown in Figure 4. The values of different radical paths based on observed VOCs are in the range of radical budget analysis reported in Beijing, Shanghai, and Guangzhou(Tan et al., 2019). The average formation rates (the numbers in Figure 4) of these four processes (OH, HO_2, RCO_3, and RO_2) derived from PIC-VOCs were higher than that from the observed VOCs. In particular, the reaction between NO and RO_2 and HO_2 increased by 1.6 and 1.3 ppb h^{-1}, respectively, which was equal to average $F(O_3)$ in the process analysis above. The contribution for the reaction between O_3 and alkenes to HO and HO_2 radical increased 14% and 6%, respectively. As for the radical sink, radical propagation, and equilibrium, they were consistent with the radical source. Furthermore, the O_3 formation from the RO_2 path based on the radical budget analysis increased 4.1% from 39.5% (observed-VOCs) to 43.6% (PIC-VOCs). These results denote that the O_3 formation process between the observed and initial VOCs showed no significant difference, while the formation rate should be underestimated if the consumed VOCs was not considered.

https://doi.org/10.5194/acp-2021-814
Preprint. Discussion started: 26 October 2021

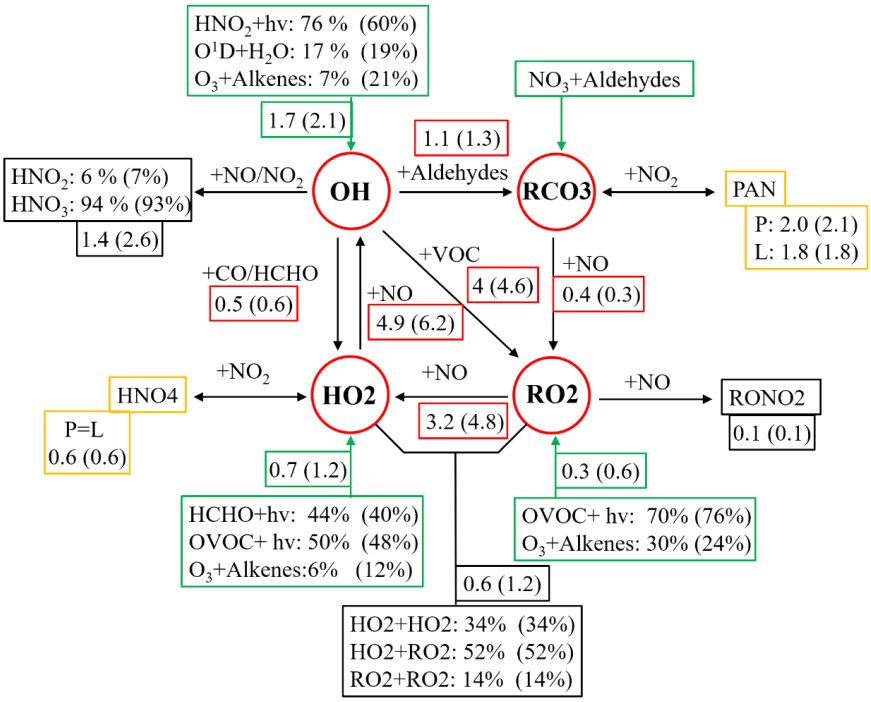

Figure 4. Comparison of the OH-HO_2-RO_2 radical budget derived from the observed and PIC-VOCs under the daytime conditions (07:00 to 19:00 LT). The green, black, red and yellow boxes denote the sources of radicals, radical sink, radical propagation, and the racial equilibrium, respectively. The numbers outside and inside the brackets in the boxes are the average formation rates (ppb h^{-1}) from the observed and PIC-VOCs.

3.4 In-situ O_3 formation process

Besides chemical processes, which can be simulated using the OBM-MCM model, the transport processes includes horizontal, vertical transportation and dry deposition processes (Tan et al., 2019) also have important influence on the O_3 concentration. Thus, the change of instantaneous ozone concentration can reflect the combination effect between the photochemical and the physical transport processes (Tan et al., 2019) . It can be expressed as,

$$\frac{dO_x}{dt} = F(O_3) + R(O_3) \quad (6)$$

where *dOx/dt* is the O_3 concentration change rate based on the measured data (ppb h^{-1}); $F(O_3)$

https://doi.org/10.5194/acp-2021-814
Preprint. Discussion started: 26 October 2021

is the net O_3 formation rate (ppb h^{-1}), and $R(O_3)$ indicates the transportation (ppb h^{-1}). The positive value of $R(O_3)$ means the inflow of O_3 with the airmass, and vice versa. O_3 was replaced with O*x* (O_3+NO_2) to correct the titration of O_3 by NO(Pan et al., 2015) .

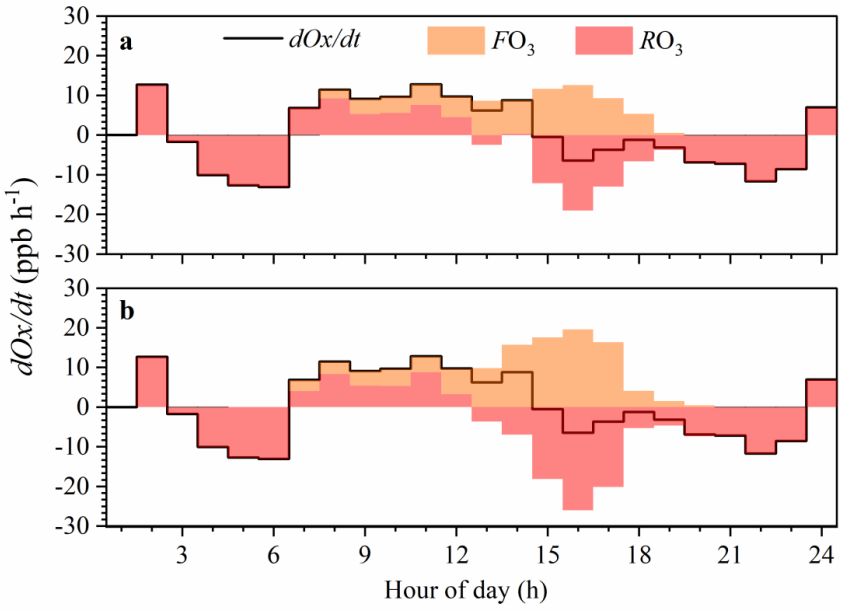

Fig. 5. The variation of O*x* concentration and formation rate on O_3 pollution episode (1st Aug). (a and b present the local ozone formation process of the measured and PIC-VOCs, respectively.)

Here shows the O_3 budget analysis occurred on a O_3 pollution episode (1st Aug). Figure 5 shows the simulated local ozone formation process based on the measured and PIC-VOCs. The hourly variation of O_3 concentrations from 19:00 to 6:00 in the next day was dominated by the regional transportation without O_3 formation, while the local photochemical O_3 formation could explain all or a part of the O_3 concentration change during the time window from 07:00 to 19:00. The d(O_3)/dt shows an increase from 07:00 to 15:00 LT. However, the d(O_3)/dt sharply changed to negative values at 16:00, which was consistent with the diurnal of O_3 (the O_3 peaks

https://doi.org/10.5194/acp-2021-814
Preprint. Discussion started: 26 October 2021

at 15:00) in Figure 1.

The average daytime F(O_3) based on the observed and photochemical initial concentration was 6.4±4.0 and 8.9±6.7 ppb h^{-1}, respectively. The photochemical O_3 formation under both conditions started at 07:00 and reached the maximum value of 12.6 and 19.6 ppb h^{-1} at 15:00, respectively. The maximum daily value of P(O_3) is higher than the urban of Japan, America, and England (Whalley et al., 2018; Ren et al., 2006; Griffith et al., 2016; Kanaya et al., 2009), lower than the suburb in Guangzhou (Lu et al., 2012), the urban and suburb of Beijing (Lu et al., 2013). Before 12:00, the O_3 formation rate based on the PIC-VOCs was slightly higher than that based on the measured ones, while both of them were within the range of 2.0~6.5 ppb h^{-1}. From 12:00 to 17:00, the O_3 formation rate based on the PIC-VOCs and the observed concentration of VOCs greatly increased due to the active photochemistry.

As shown in Figure 5, the increased O_3 concentration was larger than the local O_3 photochemical production from 07:00 to 14:00 (R(O_3) was positive). This implied an additional O_3 source from the outside regions. However, the R(O_3) was negative in the afternoon, which meant that the local O_3 formation at the measure site contributed to not only the changes of in-situ O_3 concentration but also the O_3 source of the downwind regions. This is more obviously observed in Figure 4B in the condition of the PIC-VOCs. These results illustrated that local O_3 photochemistry plays a crucial role in both the local and regional O_3 concentrations, that will be underestimated if the consumed VOCs with high reactivities are ignored.

4. Conclusions

In this study, we present the local O_3 formation process in August 2019 in Beijing based

https://doi.org/10.5194/acp-2021-814
Preprint. Discussion started: 26 October 2021

on the concentrations of the observed and PIC-VOCs. The mean diurnal profile of O_3 was unimodal with peaks at 15:00, while NO*x* and observed TVOCs showed an opposite diurnal curve, and the PICs of TVOCs showed a different diurnal curve compared with the observed one with slight increase from 14:00 to 17:00. The EKMA curve indicated that the instantaneous O_3 production was dependent on the real-time concentrations of NO*x* and VOCs, i.e., VOCs-limited regime in the morning and NO*x*-limited regime at noon. The sensitivity regime of O_3 formation could be misdiagnosed without considering the consumed VOCs, such as a VOC-limited regime (observed) shifting to a transition regime (PIC-VOCs) in the morning. The mean $F(O_3)$ based on PIC- VOCs was 3.0 ppb h^{-1} higher than that based on the measured VOCs, indicating that the underestimation of local photochemistry to local O_3 concentration could reached 36 ppb day^{-1} if the consumed VOCs were not accounted for. The radical budget analysis illustrated that the O_3 formation processes between the observed and photochemical initial VOCs showed no significant difference, but the former one underestimated the O_3 production rate obviously. Finally, the results of in-situ O_3 formation process denoted that local O_3 photochemical formation plays a key role in both local and regional O_3 concentrations. In a conclusion, our results suggest that the PIC-VOCs should be more suitable to diagnose the O_3 formation sensitivity than the observed VOCs concentrations.

https://doi.org/10.5194/acp-2021-814
Preprint. Discussion started: 26 October 2021

Author contributions: Wei Ma: Methodology, Data curation, Writing-original draft; Zemin Feng: Methodology, Investigation, Data curation, Writing-original draft; Junlei Zhan: Methodology, Investigation, Data curation; Yongchun Liu: Conceptualization, Investigation, Data curation, Writing-review & editing, Supervision, Funding Acquisition; Pengfei Liu: Methodology, Investigation, Data curation, Writing-review & editing; Chengtang Liu: Methodology, Investigation, Data curation, Writing-review & editing; Qingxin Ma: Methodology, Investigation, Data curation; Kang Yang: Methodology, Investigation, Data curation. Yafei Wang: Methodology, Investigation, Resources, Data curation; Hong He: Resources, Writing-review & editing; Markku Kulmala: Methodology, Writing-review & editing; Yujing Mu: Conceptualization, Methodology, Data Curation, Writing-review & editing. Junfeng Liu: Conceptualization, Methodology, Data curation, Writing-review & editing, Supervision.

Competing interests: The authors declare that they have no substantive conflicts of interest.

Data availability: Data are available upon request to Yongchun Liu (liuyc@buct.edu.cn)

Acknowledgements: This research was financially supported by the National Natural Science Foundation of China (41877306, 92044301, 21976190), the Ministry of Science and Technology of the People's Republic of China (2019YFC0214701), the Strategic Priority Research Program of Chinese Academy of Sciences and Beijing University of Chemical Technology.

https://doi.org/10.5194/acp-2021-814
Preprint. Discussion started: 26 October 2021

Reference

Atkinson, R. and Arey, J.: Atmospheric degradation of volatile organic compounds, Chemical Reviews, 103, 4605-4638, https://doi.org/10.1021/cr0206420, 2003.

Chen, T., Liu, J., Liu, Y., and Ma, Q. G., Yanli; Zhong,Cheng; Jiang,Haotian; Chu,Biwu; Zhang,Peng; Ma,Jinzhu; Liu,Pengfei; Wang,Yafei; Mu,Yujing; He,Hong: Chemical characterization of submicron aerosol in summertime Beijing: A case study in southern suburbs in 2018, Chemosphere, 247, https://doi.org/10.1016/j.chemosphere.2020.125918, 2020.

Cohen, A. J., Brauer, M., Burnett, R., and Anderson, H. R. F., Joseph; Estep,Kara; Balakrishnan,Kalpana; Brunekreef,Bert; Dandona,Lalit; Dandona,Rakhi; Feigin,Valery; Freedman,Greg; Hubbell,Bryan; Jobling,Amelia; Kan,Haidong; Knibbs,Luke; Liu,Yang; Martin,Randall; Morawska,Lidia; Pope,C. Arden, III; Shin,Hwashin; Straif,Kurt; Shaddick, Gavin; Thomas,Matthew; van Dingenen,Rita; van Donkelaar,Aaron; Vos,Theo; Murray,Christopher J. L; Forouzanfar,Mohammad H.: Estimates and 25-year trends of the global burden of disease attributable to ambient air pollution: an analysis of data from the Global Burden of Diseases Study 2015, Lancet, 389, 1907-1918, https://doi.org/10.1016/s0140-6736(17)30505-6, 2017.

Dang, R. and Liao, h.: Radiative Forcing and Health Impact of Aerosols and Ozone in China as the Consequence of Clean Air Actions over 2012–2017, J Geophysical Research Letters, 46, https://doi.org/10.1029/2019GL084605, 2019.

Feng, Z., De Marco, A., Anav, A., Gualtieri, M., Sicard, P., Tian, H., Fornasier, F., Tao, F., Guo, A., and Paoletti, E.: Economic losses due to ozone impacts on human health, forest productivity and crop yield across China, Environment International, 131, https://doi.org/10.1016/j.envint.2019.104966, 2019.

Gao, J., Zhang, J., Li, H., Li, L., and Xu, L. Z., Yujie; Wang,Zhanshan; Wang,Xuezhong; Zhang,Weiqi; Chen,Yizhen; Cheng,Xi; Zhang,Hao; Peng,Liang; Chai,Fahe; Wei,Yongjie: Comparative study of volatile organic compounds in ambient air using observed mixing ratios and initial mixing ratios taking chemical loss into account - A case study in a typical urban area in Beijing, Science of the Total Environment, 628-629, 791-804, https://doi.org/10.1016/j.scitotenv.2018.01.175, 2018.

Gao, Y., Li, M., Wan, X., Zhao, X., Wu, Y., Liu, X., and Li, X.: Important contributions of alkenes and aromatics to VOCs emissions, chemistry and secondary pollutants formation at an industrial site of central eastern China, Atmospheric Environment, 244, https://doi.org/10.1016/j.atmosenv.2020.117927, 2021.

Griffith, S. M., Hansen, R. F., Dusanter, S., Michoud, V., Gilman, J. B., Kuster, W. C., Veres, P. R., Graus, M., de Gouw, J. A., Roberts, J., Young, C., Washenfelder, R., Brown, S. S., Thalman, R., Waxman, E., Volkamer, R., Tsai, C., Stutz, J., Flynn, J. H., Grossberg, N., Lefer, B., Alvarez, S. L., Rappenglueck, B., Mielke, L. H., Osthoff, H. D., and Stevens, P. S.: Measurements of hydroxyl and hydroperoxy radicals during CalNex-LA: Model comparisons and radical budgets, Journal of Geophysical Research-Atmospheres, 121, 4211-4232, https://doi.org/10.1002/2015jd024358, 2016.

Han, D., Wang, Z., Cheng, J., Wang, Q., Chen, X., and Wang, H.: Volatile organic compounds (VOCs) during non-haze and haze days in Shanghai: characterization and secondary organic aerosol (SOA) formation, Environmental Science and Pollution Research, 24, 18619-18629, https://doi.org/10.1007/s11356-017-9433-3, 2017.

He, Z., Wang, X., Ling, Z., Zhao, J., Guo, H., Shao, M., and Wang, Z.: Contributions of different anthropogenic volatile organic compound sources to ozone formation at a receptor site in the Pearl River Delta region and its policy implications, Atmospheric Chemistry and Physics, 19, 8801-8816, https://doi.org/10.5194/acp-19-8801-

2019, 2019.
Kanaya, Y., Pochanart, P., Liu, Y. L., J;, Tanimoto, H., Kato, S., Suthawaree, J., Inomata, S., Taketani, F., Okuzawa, K., Kawamura, K., Akimoto, H., and Wang, Z. F.: Rates and regimes of photochemical ozone production over Central East China in June 2006: a box model analysis using comprehensive measurements of ozone precursors, Atmospheric Chemistry and Physics, 9, 7711-7723, https://doi.org/10.5194/acp-9-7711-2009, 2009.
Li, J., Wu, R., Li, Y., Hao, Y., and Xie, S. Z., Liming;: Effects of rigorous emission controls on reducing ambient volatile organic compounds in Beijing, China, Science of the Total Environment, 557, 531-541, https://doi.org/10.1016/j.scitotenv.2016.03.140, 2016a.
Li, J., Yang, W., Wang, Z., Chen, H., Hu, B., Li, J., Sun, Y., Fu, P., and Zhang, Y.: Modeling study of surface ozone source-receptor relationships in East Asia, Atmospheric Research, 167, 77-88, https://doi.org/10.1016/j.atmosres.2015.07.010, 2016b.
Li, L., An, J. Y., Shi, Y. Y., and Zhou, M. Y., R. S; Huang, C; Wang, H. L; Lou, S. R; Wang, Q; Lu, Q; Wu, J.: Source apportionment of surface ozone in the Yangtze River Delta, China in the summer of 2013, Atmospheric Environment, 144, 194-207, https://doi.org/10.1016/j.atmosenv.2016.08.076, 2016c.
Li, M., Zhang, Q., Zheng, B., Tong, D., Lei, Y., Liu, F., Hong, C., Kang, S., Yan, L., Zhang, Y., Bo, Y. S., Hang;, Cheng, Y., and He, K.: Persistent growth of anthropogenic non-methane volatile organic compound (NMVOC) emissions in China during 1990-2017: drivers, speciation and ozone formation potential, Atmospheric Chemistry and Physics, 19, 8897-8913, https://doi.org/10.5194/acp-19-8897-2019, 2019.
Ling, Z. H. and Guo, H.: Contribution of VOC sources to photochemical ozone formation and its control policy implication in Hong Kong, Environmental Science & Policy, 38, 180-191, https://doi.org/10.1016/j.envsci.2013.12.004, 2014.
Liu, Y., Yan, C., Feng, Z., Zheng, F., and Kulmala, M.: Continuous and comprehensive atmospheric observations in Beijing: a station to understand the complex urban atmospheric environment, Big Earth Data, 4, 295-321, https://doi.org/10.1080/20964471.2020.1798707, 2020a.
Liu, Y., Ni, S., Jiang, T., Xing, S., Zhang, Y., Bao, X., Feng, Z., Fan, X., Zhang, L., and Feng, H.: Influence of Chinese New Year overlapping COVID-19 lockdown on HONO sources in Shijiazhuang, Science of the Total Environment, 745, https://doi.org/10.1016/j.scitotenv.2020.141025, 2020b.
Liu, Y., Zhang, Y., Lian, C., Yan, C., Feng, Z., Zheng, F., Fan, X., Chen, Y., Wang, W., Chu, B., Wang, Y., Cai, J., Du, W., Daellenbach, K. R., Kangasluoma, J., Bianchi, F., Kujansuu, J., Petaja, T., Wang, X., Hu, B., Wang, Y., Ge, M., He, H., and Kulmala, M.: The promotion effect of nitrous acid on aerosol formation in wintertime in Beijing: the possible contribution of traffic-related emissions, Atmospheric Chemistry and Physics, 20, 13023-13040, https://doi.org/10.5194/acp-20-13023-2020, 2020c.
Lu, K. D., F. Rohrer; F. Holland, H. F., B. Bohn,T. Brauers,C. C. Chang,R. Haseler ,M. Hu,K. Kita, and , Y. K., X. Li,S. R. Lou,S. Nehr,M. Shao,L. M. Zeng,A. Wahner,Y. H. Zhang,and A. Hofzumahaus: Observation and modelling of OH and HO2 concentrations in the Pearl River Delta 2006: a missing OH source in a VOC rich atmosphere, Atmospheric Chemistry and Physics, 12, 1541-1569, https://doi.org/10.5194/acp-12-1541-2012, 2012.
Lu, K. D., Hofzumahaus, A., Holland, F., Bohn, B., Brauers, T., Fuchs, H., Hu, M., Haeseler, R., Kita, K., Kondo, Y., Li, X., Lou, S. R., Oebel, A., Shao, M., Zeng, L. M., Wahner, A., Zhu, T., Zhang, Y. H., and Rohrer, F.: Missing OH source in a suburban environment near Beijing: observed and modelled OH and HO2 concentrations in summer 2006, Atmospheric Chemistry and Physics, 13, 1057-1080, https://doi.org/10.5194/acp-13-1057-2013, 2013.

Lu, X., Chen, N., Wang, Y., Cao, W., Zhu, B., Yao, T., Fung, J. C. H., and Lau, A. K. H.: Radical budget and ozone chemistry during autumn in the atmosphere of an urban site in central China, Journal of Geophysical Research-Atmospheres, 122, 3672-3685, https://doi.org/10.1002/2016jd025676, 2017.

Ma, j. K., Jyoti;, Li, V. O. K., and Lam, J. C. K.: Effects of China's current Air Pollution Prevention and Control Action Plan on air pollution patterns, health risks and mortalities in Beijing 2014-2018, Chemosphere, 260, https://doi.org/10.1016/j.chemosphere.2020.127572, 2020.

Ma, Z., Liu, C., Zhang, C., Liu, P., Ye, C., Xue, C., Zhao, D., Sun, J., Du, Y., Chai, F., and Mu, Y.: The levels, sources and reactivity of volatile organic compounds in a typical urban area of Northeast China, Journal of Environmental Sciences, 79, 121-134, 10.1016/j.jes.2018.11.015, 2019.

Mckeen, S. A., Liu, S. C., Hsie, E. Y., Lin, X., Bradshaw, J. D., Smyth, S., Gregory, G. L., and Blake, D. R.: Hydrocarbon ratios during PEM-WEST A: A model perspective, Journal of Geophysical Research: Atmospheres, 101, https://doi.org/10.1029/95JD02733, 1996.

Monks, P. S.: Gas-Phase Radical Chemistry in the Troposphere, Chemical Society Reviews, 34, 376-395, https://doi.org/10.1039/B307982C, 2005.

Pan, X., Kanaya, Y., Tanimoto, H., Inomata, S., Wang, Z., Kudo, S., and Uno, I.: Examining the major contributors of ozone pollution in a rural area of the Yangtze River Delta region during harvest season, Atmospheric Chemistry and Physics, 15, 6101-6111, https://doi.org/10.5194/acp-15-6101-2015, 2015.

Ren, X., Brune, W. H., Mao, J., Mitchell, M. J., Lesher, R. L., Simpas, J. B., Metcalf, A. R., Schwab, J. J., Cai, C., Li, Y., Demerjian, K. L., Felton, H. D., Boynton, G., Adams, A., Perry, J., He, Y., Zhou, X., and Hou, J.: Behavior of OH and HO2 in the winter atmosphere in New York city, Atmospheric Environment, 40, S252-S263, https://doi.org/10.1016/j.atmosenv.2005.11.073, 2006.

Seinfeld and JohnH: Atmospheric chemistry and physics : from air pollution to climate change / 2nd ed, Atmospheric chemistry and physics : from air pollution to climate change / 2nd ed2006.

Shao, M., Wang, B., Lu, S., Yuan, B., and Wang, M.: Effects of Beijing Olympics Control Measures on Reducing Reactive Hydrocarbon Species, Environmental Science & Technology, 45, 514-519, https://doi.org/10.1021/es102357t, 2011.

Tan, Z., Fuchs, H., Lu, K., and Hofzumahaus, A. B., Birger; Broch,Sebastian; Dong,Huabin; Gomm,Sebastian; Haeseler,Rolf; He,Lingyan; Holland,Frank; Li,Xin; Liu,Ying; Lu,Sihua; Rohrer,Franz; Shao,Min; Wang,Baolin; Wang,Ming; Wu,Yusheng; Zeng,Limin; Zhang,Yinsong; Wahner,Andreas; Zhang,Yuanhang;: Radical chemistry at a rural site (Wangdu) in the North China Plain: observation and model calculations of OH,HO2 and RO2 radicals, Atmospheric Chemistry and Physics, 17, 663-690, https://doi.org/10.5194/acp-17-663-2017, 2017.

Tan, Z., Lu, K., Jiang, M., Rong, S., and Zhang, Y.: Daytime atmospheric oxidation capacity in four Chinese megacities during the photochemically polluted season: A case study based on box model simulation, Atmospheric Chemistry Physics, 19, 3493-3513, https://doi.org/10.5194/acp-19-3493-2019, 2019.

Tan, Z., Lu, K., Jiang, M., Su, R., Dong, H., Zeng, L., Xie, S., Tan, Q., and Zhang, Y.: Exploring ozone pollution in Chengdu, southwestern China: A case study from radical chemistry to O-3-VOC-NOx sensitivity, Science of the Total Environment, 636, 775-786, https://doi.org/10.1016/j.scitotenv.2018.04.286, 2018.

Wang, T., Xue, L., Brimblecombe, P., Lam, Y. F., Li, L., and Zhang, L.: Ozone pollution in China: A review of concentrations, meteorological influences, chemical precursors, and effects, Science of the Total Environment, 575, 1582-1596, https://doi.org/10.1016/j.scitotenv.2016.10.081, 2017.

Whalley, L. K., Stone, D., Dunmore, R., Hamilton, J., Hopkins, J. R., Lee, J. D., Lewis, A. C., Williams, P., Kleffmann, J., Laufs, S., Woodward-Massey, R., and Heard, D. E.: Understanding in situ ozone production in the

summertime through radical observations and modelling studies during the Clean air for London project (ClearfLo), Atmospheric Chemistry and Physics, 18, 2547-2571, https://doi.org/10.5194/acp-18-2547-2018, 2018.

Wiedinmyer, C., Friedfeld, S., Baugh, W., Greenberg, J., Guenther, A., Fraser, M., and Allen, D.: Measurement and analysis of atmospheric concentrations of isoprene and its reaction products in central Texas, Atmospheric Environment, 35, 1001-1013, https://doi.org/10.1016/S1352-2310(00)00406-4, 2001.

Xie, Y., Dai, H., Zhang, Y., Wu, Y., Hanaoka, T., and Masui, T.: Comparison of health and economic impacts of PM2.5 and ozone pollution in China, Environment International, 130, https://doi.org/10.1016/j.envint.2019.05.075, 2019.

Xue, L. K., Wang, T., Gao, J., Ding, A. J., Zhou, X. H., Blake, D. R., Wang, X. F., Saunders, S. M., Fan, S. J., Zuo, H. C., Zhang, Q. Z., and Wang, W. X.: Ground-level ozone in four Chinese cities: precursors, regional transport and heterogeneous processes, Atmospheric Chemistry and Physics, 14, 13175-13188, https://doi.org/10.5194/acp-14-13175-2014, 2014.

Yang, Y., Shao, M., Kessel, S., Li, Y. L., Keding;, Lu, S. W., Jonathan;, Zhang, Y., Zeng, L., Noelscher, A. C., Wu, Y., Wang, X., and Zheng, J.: How the OH reactivity affects the ozone production efficiency: case studies in Beijing and Heshan, China, Atmospheric Chemistry and Physics, 17, 7127-7142, https://doi.org/10.5194/acp-17-7127-2017, 2017.

Yuan, B., Hu, W. W., Shao, M., Wang, M., Chen, W. T., Lu, S. H., Zeng, L. M., and Hu, M.: VOC emissions, evolutions and contributions to SOA formation at a receptor site in eastern China, Atmospheric Chemistry and Physics, 13, 8815-8832, https://doi.org/10.5194/acp-13-8815-2013, 2013.

Zhan, J., Feng, Z., Liu, P., He, X., He, Z., Chen, T., Wang, Y., He, H., Mu, Y., and Liu, Y.: Ozone and SOA formation potential based on photochemical loss of VOCs during the Beijing summer, Environmental Pollution, 285, https://doi.org/10.1016/j.envpol.2021.117444, 2021.

Zhang, K., Li, L., Huang, L., Wang, Y., Huo, J., Duan, Y., Wang, Y., and Fu, Q.: The impact of volatile organic compounds on ozone formation in the suburban area of Shanghai, Atmospheric Environment, 232, https://doi.org/10.1016/j.atmosenv.2020.117511, 2020.

Zhang, K., Huang, L., Li, Q., Huo, J., Duan, Y., Wang, Y., Yaluk, E., Wang, Y., Fu, Q., and Li, L.: Explicit modeling of isoprene chemical processing in polluted air masses in suburban areas of the Yangtze River Delta region: radical cycling and formation of ozone and formaldehyde, Atmospheric Chemistry and Physics, 21, 5905-5917, https://doi.org/10.5194/acp-21-5905-2021, 2021a.

Zhang, M., Gao, W., Yan, J., Wu, Y., Marandino, C. A., Park, K., Chen, L., Lin, Q., Tan, G., and Pan, M.: An integrated sampler for shipboard underway measurement of dimethyl sulfide in surface seawater and air, Atmospheric Environment, 209, 86-91, https://doi.org/10.1016/j.atmosenv.2019.04.022, 2019.

Zhang, Q., Li, L., Zhao, W., Wang, X., Jiang, L., Liu, B., Li, X., and Lu, H.: Emission characteristics of VOCs from forests and its impact on regional air quality in Beijing, China Environmental Science, 41, 622-632, https://doi.org/10.19674/j.cnki.issn1000-6923.2021.0072, 2021b.

Zhang, S., Li, D., Ge, S., Liu, S., Wu, C., Wang, Y., Chen, Y., Lv, S., Wang, F., Meng, J., and Wang, G.: Rapid sulfate formation from synergetic oxidation of SO2 by O3 and NO2 under ammonia-rich conditions: Implications for the explosive growth of atmospheric PM2.5 during haze events in China, Science of The Total Environment, 772, 10.1016/j.scitotenv.2020.144897, 2021c.